Published online August 4, 2005

SOIL SCIENCE SOCIETY OF AMERICA
JOURNAL

VOL. 69 SEPTEMBER–OCTOBER 2005 NO. 5

Comparison of Air and Water Permeability between Disturbed and Undisturbed Soils

Atac Tuli, Jan W. Hopmans,* Dennis E. Rolston, and Per Moldrup

ABSTRACT

Although soil structure and pore geometry characteristics largely control flow and transport processes in soils, there is a general lack of experiments that study the effects of soil structure and pore-space characteristics on air and water permeability. Our objective was to determine the dependency of soil permeability on fluid content for both water and air, and compare results for both disturbed (D) and undisturbed (UD) soils. For that purpose, we first measured the water permeability (k_w) and air permeability (k_a) for several intact UD soil samples. Subsequently, the same samples were crushed and repacked into the same soil cores to create the D equivalent for the same soil material. Measurements showed large differences between D and UD samples, confirming the enormous impact of soil structure and pore-space characteristics on flow. The permeability of both fluid phases (air and water) was greatly reduced for the D samples, especially for soil air permeability due to its greater dependency on soil aggregation and structure. Soil water retention and permeability data were fitted to Campbell's and Mualem's pore-size distribution model, respectively. Regardless of soil disturbance, we showed that the tortuosity–connectivity parameter, l, for the water permeability (l_1) and air permeability (l_2) were different. This is in contrast to the general practice of using the same parameter value for both functions. The relation between l_1 and l_2 was largely controlled by soil structure and associated macroporosity properties.

Multi-fluid flow processes are governed by geometrical pore-space characteristics such as tortuosity, connectivity, and constriction. Unfortunately, most multi-fluid flow and transport modeling does not treat pore-space characteristics as a major determining factor other than by the empirical fitting of model parameters. This is so because of the inherent complexity and heterogeneity of soils, thereby making a physical interpretation of the accounting of pore-space characteristics to flow and transport very difficult. This lack of knowledge on the control of pore geometry on flow and transport has led to incidental microscopic studies that investigated flow and transport coefficients as a function of geometric soil pore-space properties (e.g., Vogel, 1997; Wildenschild et al., 2005). Others used soil physical and permeability properties to characterize macropore space and geometry (Ball, 1981a, 1981b; Blackwell et al., 1990; Schjønning et al., 2002). Assuming that the continuity of the soil pore space is organized by pore size, Ehlers et al. (1995) described the continuity of pore space using physically determined soil hydraulic properties.

To better understand the effect of pore-space geometry on flow and transport in soils, one generally assumes an idealized geometrical representation of pore space inferred from the arrangement of soil particles with a known shape. Although such porous media are a simplified version of the complex and heterogeneous reality, it is useful for studying relationships between pore structure and effective soil hydraulic properties using network and Lattice Boltzmann modeling. For example, Vogel (2000) used a network model for soils with a range of pore-size distributions and pore topologies to investigate the relationships between pore-scale processes and effective soil hydraulic properties. Although numerical experiments offer some information on the interaction between pore geometry characteristics and flow and transport processes, experimental research is required to evaluate their implication for natural soils.

Despite the different and sometimes misleading definitions in literature, Clennell (1997) presented a comprehensive review of the tortuosity concept for a range of different flow and transport processes in porous media. Although strictly a microscopic concept, pore tortuosity is applied macroscopically with pore structure and geometry embedded in the convective and diffusive transport coefficients. In the presented experimental study, we focus on convective flow only by the measurement of the saturation dependence of both air and water conductivity or permeability. Historically, air permeability has received much attention in the soil science

A. Tuli, J.W. Hopmans, and D.E. Rolston, Dep. of Land, Air, and Water Resources, Univ. of California, Davis, CA 95616, USA; P. Moldrup, Dep. of Environmental Engineering, Aalborg Univ., Sohngaardsholmsvej 57, DK-9000 Aalborg, Denmark. Received 8 Oct. 2004. *Corresponding author (jwhopmans@ucdavis.edu).

Published in Soil Sci. Soc. Am. J. 69:1361–1371 (2005).
Soil Physics
doi:10.2136/sssaj2004.0332

Abbreviations: D, disturbed; UD, undisturbed.

literature, as it may be used to characterize soil pore geometry, structure, and soil stability control as its value is determined by the geometrical arrangement of the solid particles when applied in its fluid-independent permeability form. Typical examples can be found in Ball (1981a, 1981b), where air permeability was measured as a function of air-filled porosity for UD soil samples. The objective of these studies was to evaluate differences in pore-space characteristics using basic soil physical properties and permeability measurements. In later studies, different types of predictive models were suggested for estimating air permeability in D and UD soil samples (Moldrup et al., 1998; Moldrup et al., 2001; Iversen et al., 2001). Moldrup et al. (2003) used a combination of air permeability, gas diffusivity, and soil water characteristic measurements to evaluate the effect of soil structure on pore connectivity.

Other later studies evaluated the linking between pore-space geometry and soil structure with hydraulic conductivity. Using a general model that included a tortuosity and connectivity parameter, assuming a lognormal pore-size distribution, Vervoort and Cattle (2003) investigated the relation between hydraulic conductivity and tortuosity parameters to pore space geometry and size distribution of UD soil samples, using image analysis. Although they concluded that a physical interpretation of the tortuosity and connectivity parameter cannot explicitly be determined without quantitative measures of soil structure, hydraulic conductivity and tortuosity parameters were strongly related to porosity, pore-size distribution, and mean pore size. Similarly, Tuli and Hopmans (2004) found that both pore geometry and size distribution were the main factors determining the functional relations between degree of fluid saturation and hydraulic and air conductivity. However, their results also showed that the control of pore size on convective transport is clearer for soils with a wider pore-size distribution, and that its relative contribution is much larger for hydraulic conductivity than air conductivity.

To date, we could not find any experimental study that quantified the effect of soil structure and pore fluid saturation on both air and water permeability, and that evaluated differences in air and water permeability between D and UD soil materials. In this study, we followed an approach to get a better understanding of how changes in soil structure impacts convective fluid transport by the measurement of both transport coefficients for initially UD soil samples and their disturbed equivalents for which the original soil structure was completely destroyed. Our objectives were (i) to measure air and water permeability on both UD and D forms of the same soil material; (ii) to investigate the control of soil structure on both air and water permeability as a function of fluid content through comparison of permeability measurements of both D and UD soil samples; and (iii) to determine the tortuosity–connectivity parameters of the air and water permeability model for the corresponding D and UD soil samples.

THEORY

Soil Hydraulic Functions

Due to its simpler form, we used Campbell's (1974) model for describing the soil water characteristic curve,

$$S_w = \frac{\theta}{\theta_s} = \left(\frac{h_{m,a}}{h_m}\right)^{\lambda} \qquad \text{for } h_m < h_{m,a}$$
$$S_w = 1 \qquad \text{for } h_m \geq h_{m,a} \qquad [1]$$

where θ_s is saturated water content ($L^3\,L^{-3}$), θ is volumetric water content ($L^3\,L^{-3}$), h_m is soil water matric head (L), $h_{m,a}$ is soil–water matric head at air entry (L), $\lambda = 1/b$ denotes the pore-size distribution index, and b is the slope of the soil water retention curve when using a log-log plot. We expect $h_{m,a}$ to decrease (more negative) and b to increase as the pore-size distribution becomes wider. Assuming validity of Mualem's (1976) hydraulic conductivity model, the relative permeability can be expressed by

$$k_{rw} = \frac{k_w}{k_{sw}} = S_w^l \left[\frac{\int_0^{S_w} \frac{dS_w}{h_m}}{\int_0^1 \frac{dS_w}{h_m}}\right]^2 \qquad [2]$$

where k_{rw} is the relative water permeability, k_w is the saturation-dependent soil water permeability (L^2), and k_{sw} is the saturated water permeability (L^2). In this equation, the power l defines the pore tortuosity–connectivity parameter. Substituting Eq. [1] into Eq. [2] and integrating yields the Campbell–Mualem formulation (Chen et al., 1999),

$$k_{rw} = \frac{k_w}{k_{sw}} = (S_w)^{l+2+\frac{2}{\lambda}} = (S_w)^{l+2+2b} \qquad [3]$$

As Schaap and Leij (2000) suggested, we fitted the tortuosity–connectivity parameter, rather than using a constant value of 0.5.

Relative Air Permeability

Similarly, Mualem's (1976) model can be extended to represent the relative air permeability, k_{ra}, as a function of air saturation (S_a), or

$$k_{ra} = \frac{k_a}{k_{sa}} = (1 - S_w)^l \left[\frac{\int_{S_w}^1 \frac{dS_w}{h_m}}{\int_0^1 \frac{dS_w}{h_m}}\right]^2 \qquad [4]$$

where k_a denotes the soil air permeability (L^2) and k_{sa} is the saturated air permeability (L^2). Again, substituting Eq. [1] into Eq. [4] and integrating yields (Chen et al., 1999),

$$k_{ra} = \frac{k_a}{k_{sa}} = (1 - S_w)^l \left[1 - S_w^{1+\frac{1}{\lambda}}\right]^2 = S_a^l[1 - S_w^{1+b}]^2 \qquad [5]$$

where $S_a = 1 - S_w$ (Tuli and Hopmans, 2004). In this study, we treated the tortuosity–connectivity parameter, l, in the relative air permeability function in two different ways. In the first way, relative air permeability values were predicted as a function of water saturation using the tortuosity–connectivity parameter, l_1, obtained from fitting multi-step water outflow data to Eq. [1] and [3] using parameter optimization (Hopmans et al., 2002; Chen et al., 1999; Dury et al., 1999; Miller et al., 1998). In the second case, instead of using a common parameter value for both air and water permeability, the tortuosity–connectivity parameter of the relative air permeability equation (Eq. [5]) was optimized independently using measured air permeability data defined by l_2.

Tortuosity and Connectivity

Since flow and transport processes are largely controlled by the arrangements of the pores and soil particles within the soil matrix, we focus in this study on effect of the l parameter on permeability, as defined by Eq. [2] and [4]. Even though it can be argued that this tortuosity–connectivity parameter is treated as a fitting parameter, and no specific relationship to the soil's physical and pore-space geometry is suggested, it is worthwhile to investigate differences in parameter values between UD and D soil samples, as soil disturbance will greatly affect pore-space geometrical characteristics. To better quantify the saturation dependence of soil tortuosity, we assumed that tortuosity-connectivity coefficient or tortuosity for water (τ_w) and air (τ_a) phase can be defined by (Vervoort and Cattle, 2003),

$$\tau_w = S_w^{l_1} \qquad \tau_a = S_a^{l_2} \qquad [6]$$

where τ corresponds with the pore geometry term, G, of Tuli and Hopmans (2004).

MATERIALS AND METHODS

Soil Sample Preparation

We initially collected 18 UD soil samples using 8.25-cm i.d., 6 cm long core samplers for our experiments (Tuli et al., 2001a). The UD soil samples were soaked in 0.01 M $CaCl_2$ solution to prevent swelling and dispersion to saturate the samples. Upon saturation, soil columns were placed on a rigid screen so that saturated hydraulic conductivity of soil samples could be measured using the constant head method (Klute and Dirksen, 1986). After completing the saturated hydraulic conductivity measurements, the measured values, K_{sw}^m, were converted to saturated water permeability, k_{sw}^m at room temperature of 25°C. Subsequently, the soil samples were assembled in Tempe pressure cells for estimation of the soil hydraulic functions using multi-step outflow experiments (Eching et al., 1994; Tuli et al., 2001b). Each cell included a vertically placed 6-mm diam. miniature tensiometer, with the cup placed in the center of the soil sample. The samples were resaturated with the 0.01 M $CaCl_2$ solution through the bottom porous membrane assembly, to ensure good contact between the soil sample and the porous membrane.

After completion of all experiments for the UD soil samples, all UD samples were oven-dried at 105°C overnight to determine soil water content at corresponding pressure steps. Each oven-dried UD sample was crushed and sieved through a 2-mm sieve (Singer, 1986). The sieved soils were packed into the same core samplers as the corresponding UD sample, at near equal bulk densities. Identical experimental procedures were followed for the D samples. The general soil properties such as sampling depth, soil texture, and organic matter content of the soils are given in Table 1. The main soil physical properties for each soil sample, both UD and D are presented in Table 2. The number of samples was reduced to 13, eliminating those samples for which soil water matric head data were erroneous because of the malfunctioning of pressure transducers during the outflow experiment of either the D or UD soil samples.

Soil Hydraulic Functions

The soil hydraulic functions for each soil sample were measured using the multi-step outflow method, with hydraulic parameters estimated using inverse modeling technique (Eching et al., 1994; Hopmans et al., 2002). Relative to the sample's initial saturated condition, the multi-step outflow method uses the measured changes in cumulative drainage and soil-water matric pressure as caused by changing applied gas pressure, to optimize the hydraulic parameters. For all soil samples, we applied an initial pressure step of 4.5 kPa to ensure that the air entry value of the soil was exceeded before executing the multi-step experiment (Hopmans et al., 2002). We only applied four subsequent pressure steps due to long experimental time requirements. Although we tried to apply identical air pressure steps for all samples, some samples only drained small water volumes in response to early pressure steps. If this was the case, we stepwise increased pressure, starting at near-saturation until significant drainage was achieved. Generally, for UD soil samples, the external applied pressure steps were: 8, 15, 35, and 50 kPa, whereas for the D soil samples, applied pressure steps were 15, 20, 35, and 50 kPa. The first two pressure steps were different between the two sample types, to ensure sufficient air permeability for the D soil samples.

Measurements were first conducted for the set of UD soil samples. Between each increment of pressure, the soil samples

Table 1. Sampling depth, soil texture, textural class, and organic matter content (OM) of soil samples.

Sample	Depth	Soil texture: Sand	Silt	Clay	Textural class†	OM
	cm	g kg^{-1}				g kg^{-1}
41	25	540	330	130	SL	5.2
44	50	350	550	100	SiL	5.1
59	25	410	420	170	L	7.9
127	25	290	510	200	SiL	11.4
128	50	250	570	180	SiL	9.5
129	25	340	460	200	L	11.1
131	25	290	510	200	SiL	11.1
132	50	260	550	190	SiL	10.5
134	50	300	490	210	L	11.2
137	25	390	430	180	L	10.7
139	25	360	440	200	L	10.9
142	50	230	620	150	SiL	7.6
143	25	440	370	190	L	10.3

† SL, sandy loam; SiL, silt loam; L, loam.

Table 2. Some physical properties of disturbed and undisturbed soils.†

Sample	Bulk density ρ_b	Porosity ø	θ_s^m	k_{sw}^m
	g cm^{-3}	cm^3 cm^{-3}		cm^2
		Undisturbed soil samples		
UD41	1.53	0.421	0.393	1.141E-09
UD44	1.34	0.493	0.447	2.320E-09
UD59	1.64	0.381	0.378	1.987E-10
UD127	1.45	0.452	0.419	7.484E-10
UD128	1.29	0.514	0.414	6.330E-09
UD129	1.49	0.439	0.406	7.497E-09
UD131	1.40	0.471	0.403	4.991E-09
UD132	1.43	0.460	0.412	1.612E-09
UD134	1.47	0.444	0.402	2.259E-10
UD137	1.49	0.439	0.412	3.089E-09
UD139	1.44	0.456	0.405	2.773E-09
UD142	1.20	0.548	0.501	1.458E-08
UD143	1.46	0.450	0.446	2.874E-09
		Disturbed soil samples		
D41	1.48	0.443	0.437	6.288E-10
D44	1.30	0.508	0.447	1.839E-09
D59	1.53	0.421	0.421	6.927E-11
D127	1.40	0.470	0.465	1.252E-10
D128	1.28	0.515	0.467	3.521E-10
D129	1.47	0.444	0.442	1.217E-10
D131	1.39	0.476	0.469	1.518E-10
D132	1.42	0.466	0.462	2.217E-10
D134	1.46	0.449	0.449	6.194E-11
D137	1.47	0.446	0.446	2.857E-10
D139	1.42	0.464	0.442	4.076E-10
D142	1.18	0.556	0.556	1.402E-09
D143	1.44	0.457	0.425	1.593E-10

† UD and D signify for Undisturbed and Disturbed soil samples, respectively; Superscript "m" signifies measured value.

were allowed to equilibrate with the current applied pressure. After zero drainage was achieved, the UD soil samples were removed from the Tempe cells and the air permeability was measured at the corresponding equilibrium soil water saturation value. In addition, we measured electrical conductivity and gaseous diffusion, however, these results will be reported in a subsequent paper. Thus, for each soil water saturation value, both water permeability and air permeability were measured for the same soil sample. Soil samples were weighed at the beginning and end of each measurement, to ensure that there was no loss of water between measurements. The UD soil samples were reassembled into Tempe pressure cells after completing the air permeability measurements. To ensure hydraulic contact between the soil sample and the porous nylon membrane after reassembling the Tempe cell, a small volume of $CaCl_2$ solution was poured on the nylon membrane, after which the equilibrium external pressure was applied for some time before the next pressure step was applied. When air permeability measurements were completed for all soil samples at the specific applied pressure, the next pressure step was applied to all reassembled samples simultaneously. These same procedures were repeated for subsequent pressure steps. At the conclusion of the experiment, soil samples were oven-dried from which the water content at the last pressure step was determined. The parameters required for soil hydraulic functions ($h_{m,a}$, b, K_{sw}, and l_1) were estimated using the SFOPT optimization program (Tuli et al., 2001b; Hopmans et al., 2002). Uniqueness issues related to the multi-step outflow method and SFOPT were specifically addressed in Hopmans et al. (2002). Parameter uniqueness was evaluated using three different sets of initial parameters for each optimization. Fitted saturated hydraulic conductivity values, K^o_{sw} were converted to saturated (intrinsic) water permeability, k^o_{sw} values using the viscosity and density values of a 0.01 *M* $CaCl_2$ solution at 25°C.

Air Permeability

The air permeability of each UD and D sample was measured by the constant pressure-gradient method (Janse and Bolt, 1960). We followed the same experimental procedures of Tuli and Hopmans (2004). To obtain relative air permeability at corresponding volumetric air content values, a reference air permeability value was needed. Due to experimental difficulties in measuring air permeability for dry soil conditions (Tuli and Hopmans, 2004), instead we substituted the optimized air permeability values, k^o_{sa}, at air saturation, as a reference point for each soil sample. We did not assume that the intrinsic permeability of air was identical to that of water, because of differences in the slip boundary near the pore wall between water and air flow (Bear, 1972). Thus, the air permeability values, k^o_{sa}, at air filled porosity, and l_2 were estimated by fitting these parameters with the model given in Eq. [5] to measured air permeability data. In these optimizations, we used the retention parameter b that was obtained from the multi-step optimization. The corresponding water saturation values were measured from drainage volumes and oven-drying of the soil samples at the completion of the outflow experiment.

Data Analysis

As pointed out earlier, we first used the optimized l_1 parameter, rather than simply using a constant value of 0.5 to describe the relative air permeability function, Eq. [5] (Schaap and Leij, 2000). As an alternative, we hypothesized that the tortuosity–connectivity parameter, l, is different for the water and air permeability functions. Thus, we fitted the tortuosity–connectivity parameter, l_2 and saturated air permeability, k^o_{sa} to Eq. [5], by minimizing residuals between measured and fitted air permeability at corresponding water saturation values, using the objective function (O)

Table 3. Optimized parameters and RMSE values for fitted relative soil air and water permeability functions.†

Sample	$h_{m,a}$	b	λ	l_1	l_2	k^o_{sw}	k^o_{sa}	$RMSE_1$	$RMSE_2$
	cm					cm^2			
				Undisturbed soil samples					
UD41	46.93	5.23	0.19	0.339	0.835	1.938E-10	7.272E-08	0.1037	0.0323
UD44	58.96	4.57	0.22	12.219	1.372	1.546E-09	2.684E-07	0.1121	0.0656
UD59	45.78	8.93	0.11	6.164	1.307	7.480E-10	2.772E-07	0.0489	0.0283
UD127	38.72	12.11	0.08	8.962	1.796	5.838E-09	1.268E-06	0.0397	0.0151
UD128	43.29	6.84	0.15	0.0002	0.084	1.834E-11	1.300E-07	0.1742	0.0571
UD129	51.89	7.76	0.13	9.701	1.303	4.203E-10	9.045E-07	0.0371	0.0338
UD131	52.97	6.87	0.15	0.020	1.301	3.997E-11	2.629E-06	0.2557	0.0286
UD132	56.49	6.00	0.17	0.003	2.454	7.842E-11	4.483E-06	0.2562	0.0458
UD134	50.58	9.58	0.10	10.186	1.434	2.071E-10	6.139E-07	0.0346	0.0197
UD137	46.86	6.40	0.16	4.709	1.433	2.327E-10	4.145E-07	0.0557	0.0253
UD139	53.37	4.69	0.21	6.369	0.887	1.885E-10	6.796E-07	0.1030	0.0482
UD142	51.38	3.33	0.30	0.003	0.007	8.070E-12	6.072E-07	0.0617	0.0617
UD143	42.29	8.35	0.12	10.422	0.490	2.313E-10	1.749E-07	0.1979	0.0438
				Disturbed soil samples					
D41	53.46	6.44	0.16	0.00013	0.871	1.717E-10	4.994E-08	0.2626	0.0454
D44	47.58	5.47	0.18	0.00286	0.885	5.642E-11	3.911E-08	0.1986	0.0514
D59	76.75	20.00	0.05	0.11497	2.300	3.728E-12	6.099E-07	0.3496	0.0438
D127	55.93	15.51	0.06	0.000010	5.005	2.083E-12	8.692E-07	0.4934	0.1197
D128	50.20	6.81	0.15	0.88205	2.507	1.452E-10	3.587E-07	0.0669	0.0385
D129	51.61	11.20	0.09	0.03323	2.619	4.738E-11	8.270E-07	0.2659	0.0248
D131	37.24	10.76	0.09	0.00104	4.909	4.784E-11	6.032E-07	0.4425	0.0440
D132	45.48	10.03	0.10	0.00323	2.625	6.128E-11	1.208E-07	0.4098	0.0278
D134	52.77	12.04	0.08	0.00025	2.622	8.520E-11	3.752E-07	0.3813	0.0243
D137	50.03	9.37	0.11	0.01216	2.643	2.992E-11	1.013E-07	0.4002	0.0313
D139	70.18	7.59	0.13	0.00415	2.603	1.546E-11	8.728E-07	0.3330	0.0263
D142	34.44	7.90	0.13	0.00223	4.134	1.042E-09	5.410E-07	0.4786	0.0609
D143	71.43	9.18	0.11	0.00053	7.728	1.795E-11	8.494E-06	0.4477	0.0817

† Superscript "o" signifies optimized value.

$$O(\mathbf{b}) = \sum_{i=1}^{I} [k_a^*(S_w) - k_a(S_w,\mathbf{b})]^2 \quad [7]$$

where k_a^* (S_w) and k_a (S_w) denote the measured and fitted air permeability value, respectively. The vector **b** contains values of the optimized parameters, k_{sa}^o and l_2. Excel software (Microsoft Corp., WA) was used for the parameter fitting (Wraith and Or, 1998).

The performance of the model for the two cases was evaluated by the root mean squared error (RMSE) using

$$\text{RMSE} = \sqrt{\frac{\sum_{j=1}^{J}\sum_{i=1}^{I(j)}[y_j^*(S_{w,i}) - y_j(S_{w,i})]^2}{N}}, \quad [8]$$

where $y_j^*(S_{w,i})$ and $y_j(S_{w,i})$ denote the measured and fitted retention or permeability data, respectively, i denotes measurement number and j represents the measurement type. Specifically, $j = 1$ for k_w, $j = 2$ for k_a, and $j = 3$ for S_w (h_m). Hence, $J = 3$ (soil water retention, water permeability, and air permeability), and $I(j)$ and N define the total number of measurements within measurement type and total number of measurements [$N = I(j) \times J$], respectively. The two cases in Table 3 are represented by RMSE_1 (only with parameter l_1) and RMSE_2 (with parameters l_1 and l_2). Among a total of 13 samples, we selected 9 samples randomly for presentation.

RESULTS AND DISCUSSION

Soil Water Characteristics

The soil water retention curves for both the D (dashed lines) and UD soil samples (solid lines), as estimated from the multi-step outflow experiment, are shown in Fig. 1, whereas the corresponding parameters for Eq. [1] are presented in Table 3. The open (D) and solid (UD) symbols in Fig. 1 denote the independently measured equilibrium soil water retention data, after reaching zero drainage at each of the applied gas pressures. Although the agreement between these independent retention data and the optimized soil water retention curves is generally very good, some discrepancies are present for the D samples at the final applied pressure of 50 kPa. However, with the exception of Sample 44, the comparison clearly demonstrates large differences between the D and UD soil samples. Since the soil textures of both samples are identical, differences can only be attributed to the control of soil structure on soil water retention. Differences in water saturation and porosity are attributed to the slightly lower bulk density values of the packed D samples. We note that differences in the shape of the retention curves between the

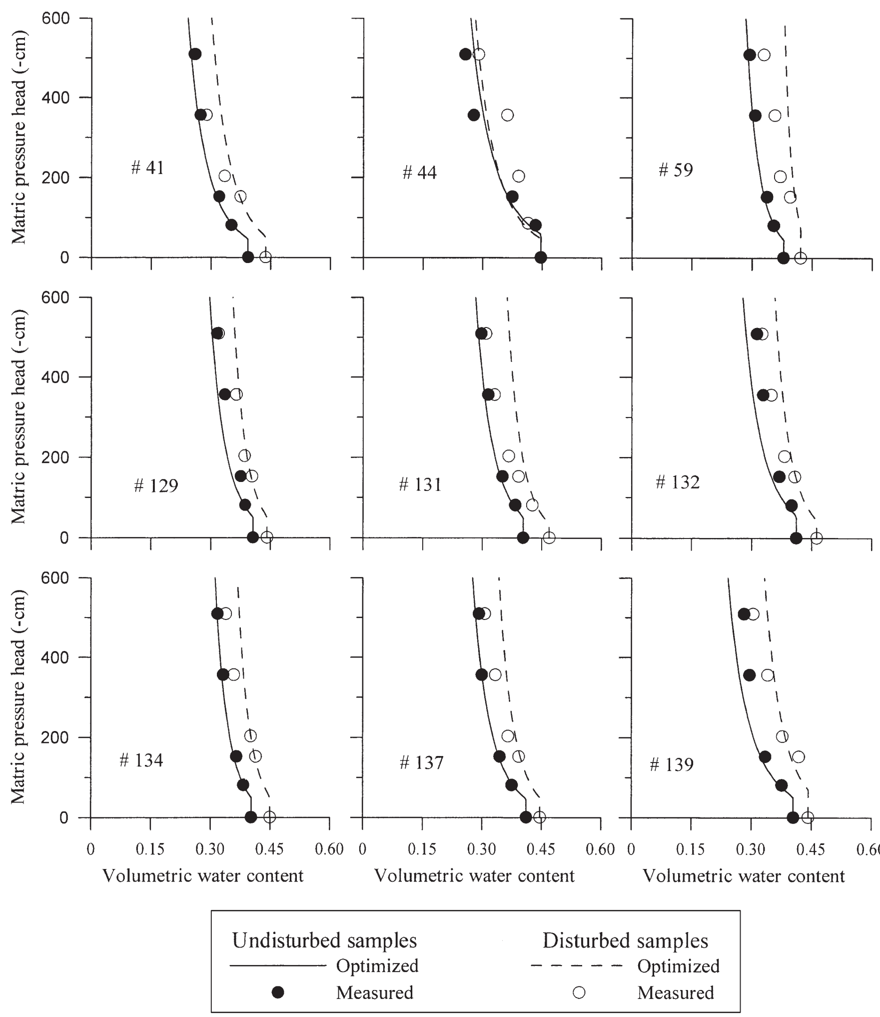

Fig. 1. Soil water characteristic curves and independently measured equilibrium water content values for the undisturbed and disturbed soil samples.

D and UD samples occurs primarily in the low matric potential head range (1–35 kPa), as would be expected if differences are caused by the lack of macropores (interaggregate pore space) in the D samples. We note that drainage for most D samples was almost absent and much smaller than for the UD samples after the first pressure step (8 kPa). Therefore, we increased the applied pressure to 15 kPa, and excluded the 8-kPa pressure data point for the D samples. Moreover, the optimization results in Table 3 indicate that the optimized air entry pressure values ($h_{m,a}$) for the D samples were higher for most cores than for the UD samples. The removal of soil structure is expected to create a narrower pore-size distribution, thereby reducing the optimized λ values of the retention functions of the D samples. Since the smaller soil pores control soil water retention at the lowest matric head values, soil water retention is controlled by soil texture only. Therefore, we expect the retention curves of both the D and UD soil samples to converge to similar values as the matric head decreases. The data in Fig. 1 indeed confirm this expectation.

Soil Air and Water Permeabilities

Whereas the soil's hydraulic conductivity depends on attributes of both the soil matrix and the moving fluid (Bear, 1972; Hillel, 1998), the soil's permeability is solely a function of the soil's pore space characteristics, that is, porosity, pore-size distribution, pore shape, pore tortuosity, and connectivity. Therefore, to evaluate the effects of soil structure on transport, we compared differences in permeability values to air and water.

The first relevant comparison would be to evaluate differences in the measured saturated water permeability, k_{sw}^{m} as presented in Table 2. As shown, the UD k_{sw}^{m} values are almost one order of magnitude larger than the corresponding values for the D samples. These large differences clearly illustrate the contribution of macropores to water flow in the UD soil samples. The same clear trend also occurred for the optimized permeability values, as listed in the seventh column of Table 3, with optimized saturated water permeability values, k_{sw}^{o} significantly smaller than the k_{sw}^{m} values for both the D and UD samples. The lower optimized permeability or conductivity values at saturation than corresponding measured values is a consequence of the extrapolation of the unsaturated conductivity function for a strictly unsaturated outflow experiment (Hopmans et al., 2002).

Figure 2 presents a comparison of soil water permeability values of D and UD soil samples as a function of volumetric water content. The presented maximum water permeability values correspond to the k_{sw}^{o} values of Table 3. The other plotted data were obtained from

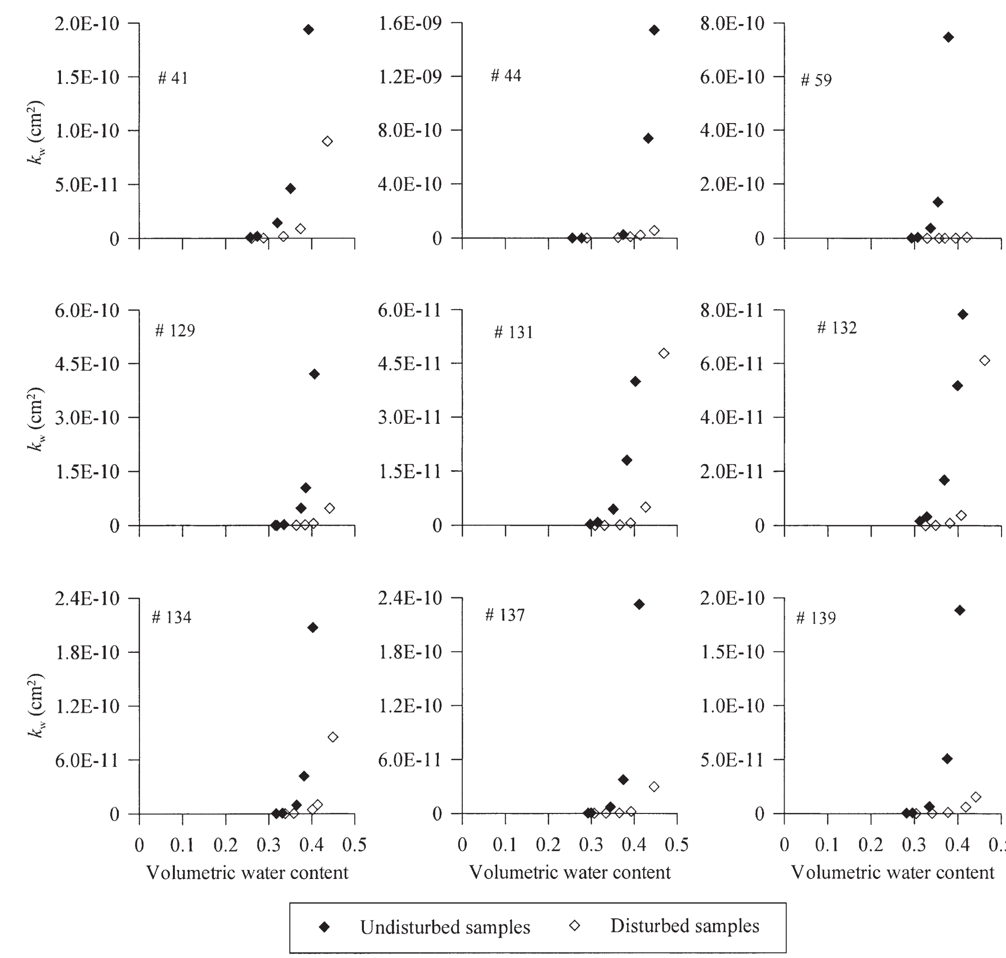

Fig. 2. Measured water permeability values as a function of volumetric water content for the undisturbed and disturbed soil samples.

substitution of the equilibrium water content values at the corresponding applied pressure steps into Eq. [3], and using the optimized hydraulic function parameters of Table 3. Specifically, we note that differences between water permeabilities of D and UD samples are quite significant in the high water content range. This is expected because of the likely contribution of macropores to water permeability for the UD soil cores (solid symbols). Overall, the high permeability of soils to water near saturation is probably due to macropore flow (Iversen et al., 2001), whereas low permeability to water occurs in the smaller pores. After the water-filled macropores are drained after the 35-kPa external pressure application, permeability of the UD soil samples decreases drastically for both sample types. Thus, water permeability values between the UD and D samples converge at the higher applied pressures, because water flow is limited to the smaller pore sizes only.

Figure 3 presents the measured air permeability of the D and UD soil samples at equal volumetric air content values as for the water permeability graphs in Fig. 2. The volumetric air content was calculated from the difference between the sample's porosity and independently measured volumetric water content value. No attempt was made to measure the soil's air permeability at water saturation, assuming air phase continuity was zero then. Except for samples 41 and 59, the results show a large increase in air conductivity across the air content range for the UD sample; again confirming the relevance of the macropores to air permeability. We hypothesized that the increased separation between the air permeability values of the UD and D samples is in part the result of increased pore connectivity for the UD samples. We note that the increase in air permeability for the D soils is much more gradual than for the UD samples, implying that changes in pore connectivity–tortuosity with air saturation is much more drastic for the UD samples.

In general, the results in Fig. 2 and 3 confirm that differences in permeability data between UD and D soils is mostly governed by soil structure and macroporosity as suggested by Blackwell et al. (1990). Therefore, permeability models should account for soil structural variations between soils (Moldrup et al., 1998, 2001). We also note that the soil's permeability values to air are generally larger than for water at similar fluid phase content values (Bear, 1972; Iversen et al., 2001; Tuli and Hopmans, 2004; Chen et al., 1999), regardless of soil structure effects.

While many analytical models have been proposed to characterize constitutive relationships based on pore geometry parameters obtained from soil hydraulic functions (e.g., Chen et al., 1999), only few experimental studies have investigated the validity of these coupled relationships between relative air permeability, water permeability, and fluid saturation, using equivalent model parameters (Moldrup et al., 2001; Tuli and Hopmans, 2004). None of these studies compared D with UD soil samples to specifically address the effect of soil structure on the constitutive relationships. In contrast,

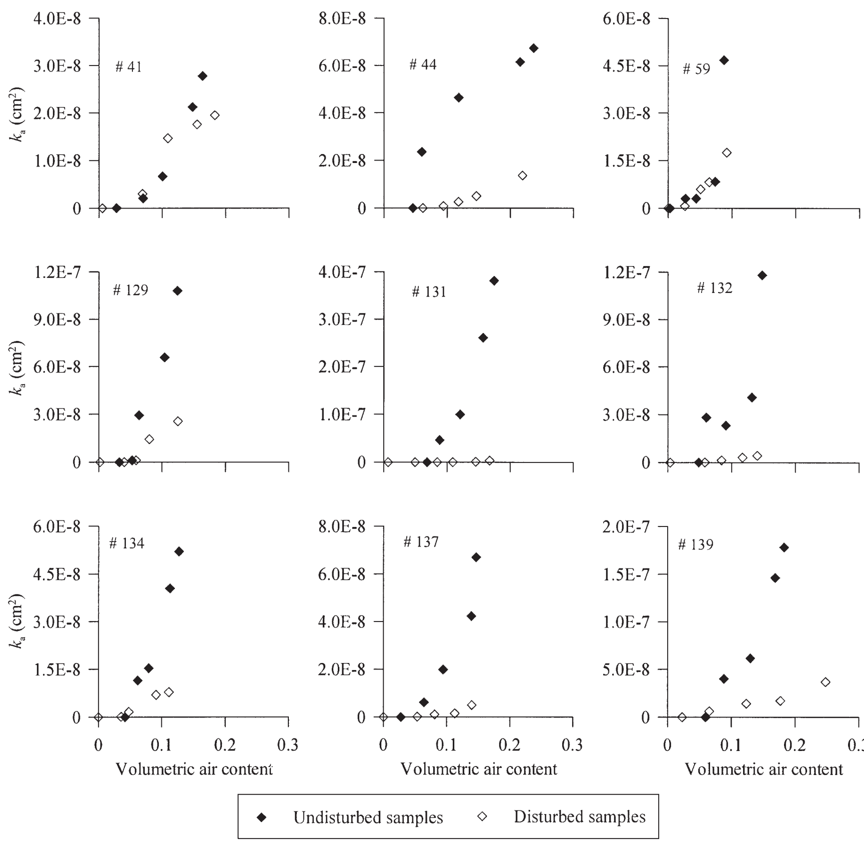

Fig. 3. Measured air permeability values as a function of volumetric air content for the undisturbed and disturbed soil samples.

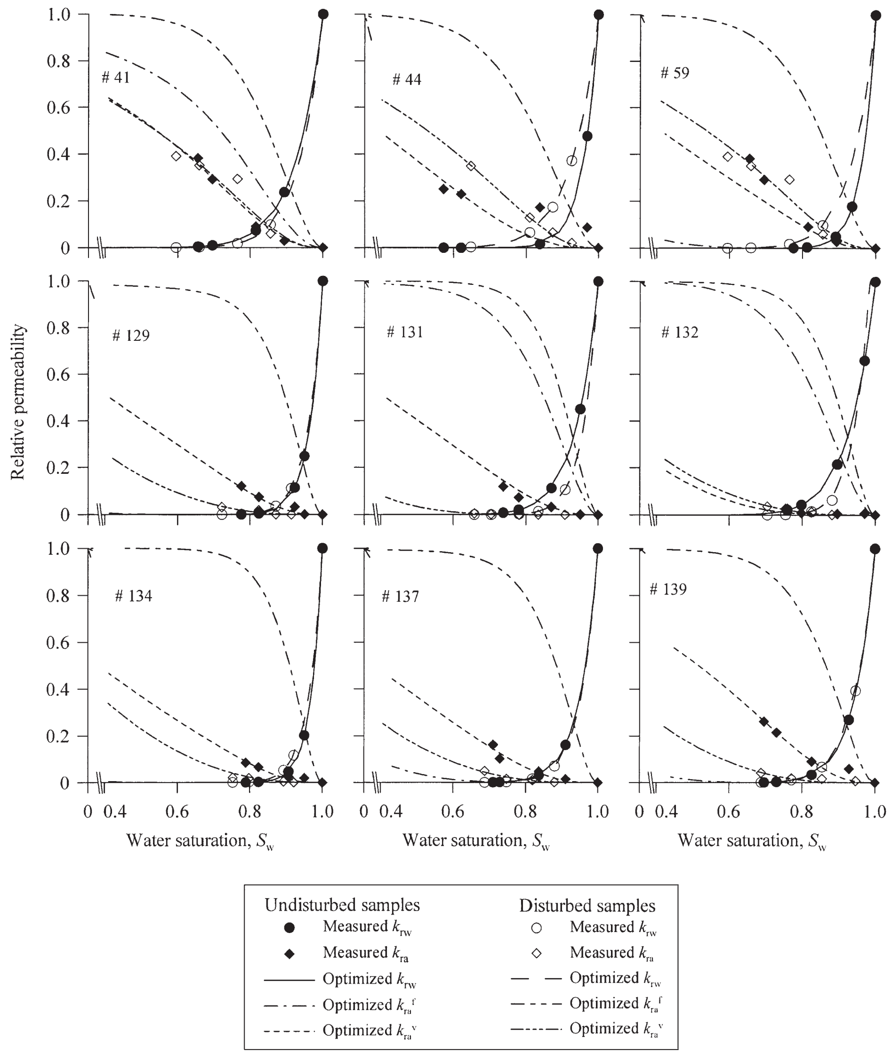

Fig. 4. Relative permeability of undisturbed and disturbed soil samples as a function of water saturation ($S_w = \theta/\theta_s$). k_{ra}^f and k_{ra}^v represent the optimized relative air permeability with tortuosity–connectivity parameter from multistep outflow optimization (l_1) and from fitting to independently measured air permeability data (l_2) using Eq. [5], respectively.

we present in Fig. 4 the relative permeability of soil to air and water as a function of water saturation, S_w, for both D and UD soil samples. The agreement between measured and optimized relative water permeability values (solid and open circles) is excellent for both D and UD samples. This is expected since both are obtained from the multi-step outflow experiments. Moreover, since the relative permeability function largely removes the soil structure effect by dividing by the fluid-specific saturated values, the general trend shows that there is little difference between relative water permeability functions of the D and UD samples. The comparison is more complicated for the fitted relative air permeability curves, as the tortuosity–connectivity parameter, l, was obtained in two different ways. For case 1, the l value for the permeability relationships of water and air are identical, and were obtained from the simultaneous optimization of soil water retention and water permeability functions. This parameter l_1 was directly used in relative air permeability function, k_{ra}^f where the superscript ‘f’ indicates that l was fixed. The corresponding functional relationships in Fig. 4 provide a rather unsatisfactory fit, largely overestimating the air permeability data for all D soil samples. For Case 2, instead the connectivity–tortuosity parameter for the air permeability function was independently fitted to measured air permeability data, to yield l_2 with the relative air permeability values obtained from the ratio between measured air permeability and optimized saturated air permeability, k_{sa}^o. In contrast, the corresponding relative air permeability curve, k_{ra}^v with the superscript ‘v’ denoting variable l provides an excellent fit to the measured data. The RMSE values for the combined fitting of all three hydraulic functions for both Cases 1 and 2 are listed in last two columns of Table 3. Since the contribution of soil water retention and relative water permeability function to the listed RMSE values is the same for both cases, the much smaller RMSE values for Case 2 are a consequence of the much better fit of the relative air permeability data. Thus, we conclude from these results that the common practice of using similar l parameter values for both air and water permeability is incorrect.

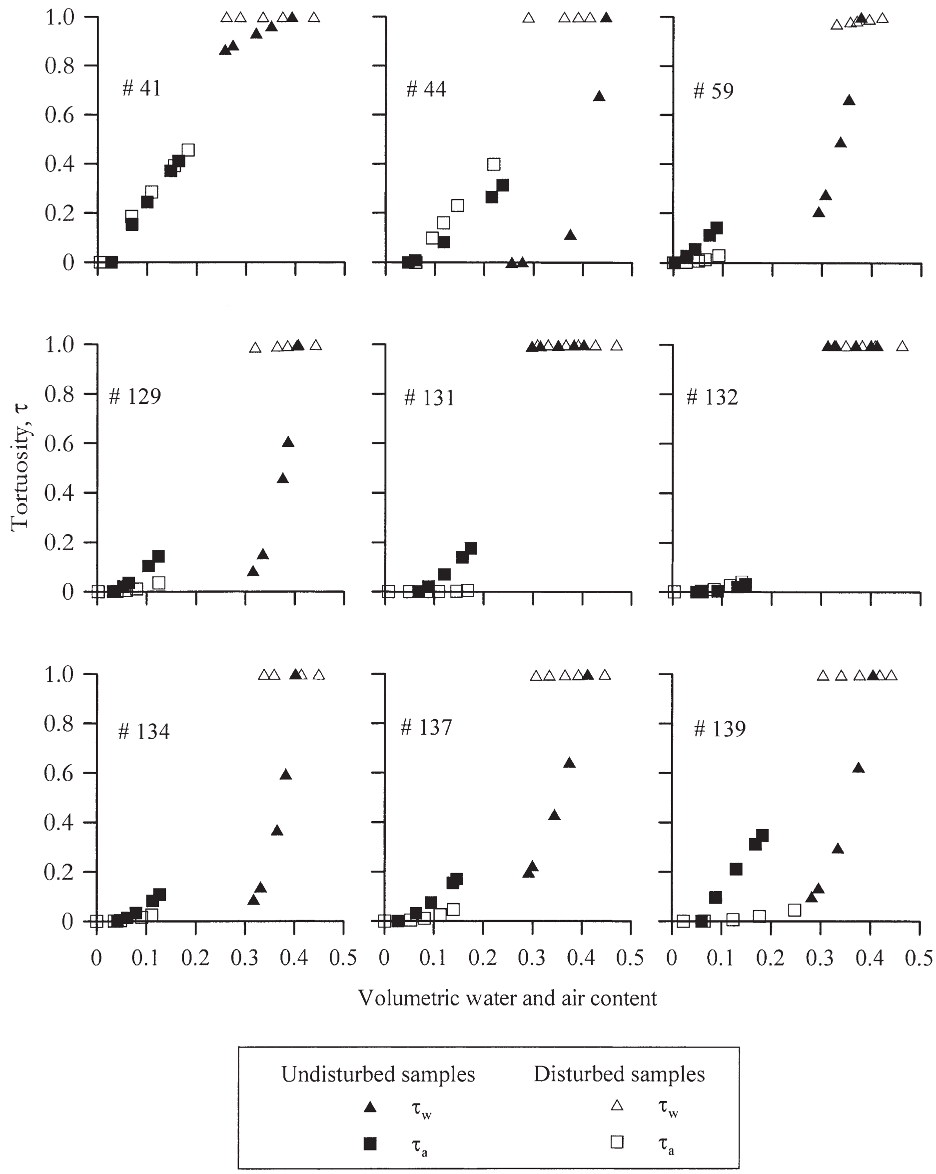

Fig. 5. Air and water tortuosity as a function of volumetric air and water content for undisturbed and disturbed soil samples.

Evidence was also presented by Luckner et al. (1989) and Tuli and Hopmans (2004).

Pore Geometry Analysis

We show the pore tortuosity–connectivity coefficient, τ, as a function of water or air content, for both the D and UD soil samples in Fig. 5. In this discussion, the tortuosity concept is based on the definition of Bear (1972), where $\tau = (L/L_e)^2 < 1$, and high connectivity corresponds to large τ values. Differences in τ between D and UD samples for the water phase (triangles) are consistent, except for Samples 131 and 132. The larger τ values for the D samples near water saturation are consistent with the smaller l values in Table 3, and are a consequence of the macroporosity and soil structure effects, resulting in a sudden drop in τ after the larger water-filled connecting pores are being drained as in UD samples for water phase. The fluid saturation value corresponding with discontinuity in the τ data, agrees with the continuum percolation threshold concept (Hunt and Gee, 2002a, 2002b; Hunt, 2004), defining a critical volume of water to maintain fluid permeability. Since the D samples lack soil structure, the decrease in τ and thus pore connectivity is much more gradual, and a threshold is much more difficult to define. Similar to water phase, the effect of soil structure on pore geometry and the l parameter for air permeability (squares) is demonstrated in Fig. 5. In general, we find that τ is larger for the UD samples (solid squares), corresponding with smaller l_2-values (Table 3), with the exception of Sample 44.

Using the notation of Tuli and Hopmans, (2004), the pore-geometry term, G_j or τ_j in Eq. [6] accounts for increasing flow paths, pore connectivity and pore constriction of the pore space. We assume that pore geometry term is an exponential function of fluid saturation, with the exponent l, describing the pore tortuosity–connectivity coefficient on permeability. As pointed out

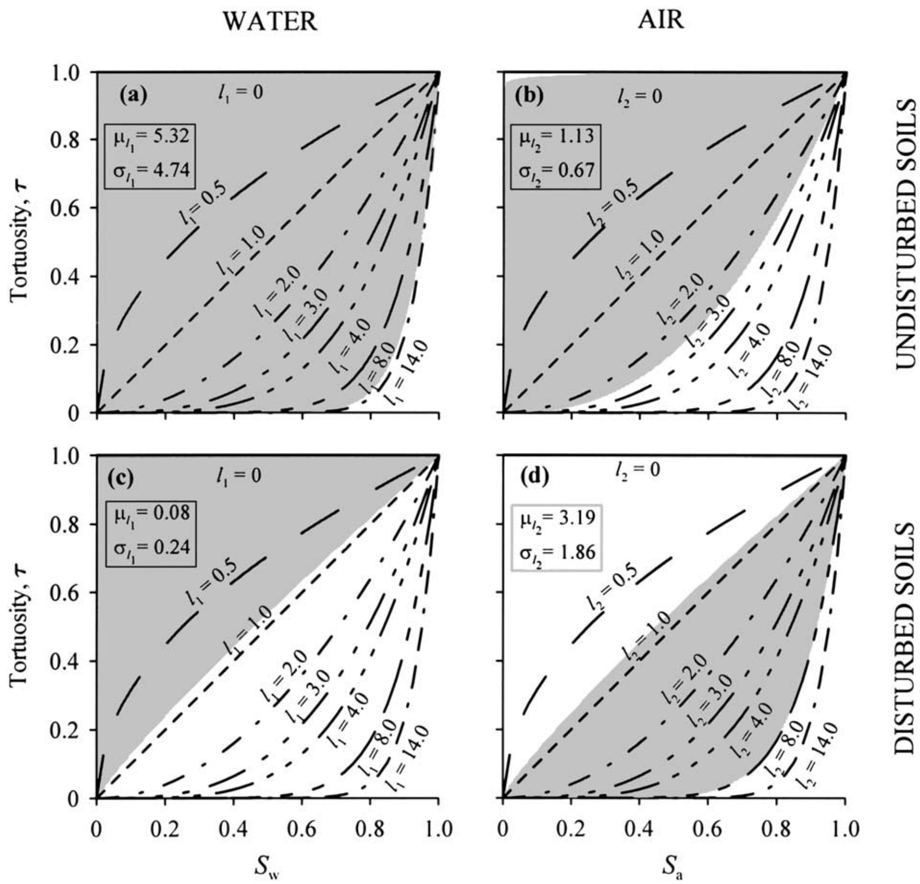

Fig. 6. Sensitivity of tortuosity (τ) on tortuosity–connectivity parameters, l_1 and l_2 of undisturbed soil samples for (a) water and (b) air phase and of disturbed soil samples for (c) water and (d) air phase, respectively. Shaded areas in each figure represent range of l_1 and l_2 parameters (Table 3) of water and air phase, respectively, for corresponding undisturbed and disturbed soil samples.

in Tuli and Hopmans (2004), near-zero l values indicate that permeability is mostly reduced in the low saturation range, with large l values reducing permeability near saturation. In this paper, l_1 and l_2 describe the connectivity and tortuosity effects on water and air permeability, respectively. Figure 6 summarizes our results, by presenting differences in the range of fitted l values using shaded areas for UD (Fig. 6a and b) and D (Fig. 6c and d) soil samples, showing the effect of l_1 (water) and l_2 (air) on τ as a function of degree of saturation. The same four figures also include the mean (μ) and standard deviation (σ) values for the respective sets of l.

Comparing l values for the UD samples (Fig. 6a and b), we find that the tortuosity–connectivity coefficient is generally larger for water as compared with air permeability ($l_1 > l_2$). This result confirms that for UD soils, water permeability is controlled by the connectivity of the macropores at near saturation. The opposite is true for the D soils (Fig. 6c and d), where generally $l_1 < l_2$, indicating that the air permeability for these soils is mostly controlled by pore connectivity (Tuli and Hopmans, 2004).The smaller l_1 values for water permeability for the D soils imply that pore-size distribution is an important factor controlling the water permeability even though connectivity of water phase is already established at higher water saturations (Fig. 6c). Although not as clear, the larger l_2 values for the D samples are an indication of a threshold value of air permeability, with k_{ra} remaining low due to the low connectivity of air phase at near water saturation, but increasing rapidly as the threshold value of air saturation is exceeded after drainage of the structural macropores, establishing connectivity of the air phase (Fig. 6d).

CONCLUSIONS

Our results clearly demonstrate the effect of soil structure on pore geometrical characteristics and on soil water retention, unsaturated hydraulic conductivity, and air permeability. Both the soil water characteristics and water permeability curves were determined from multistep outflow measurements, whereas the saturation dependence of air permeability was determined from constant pressure-gradient permeameter measurements. Disturbed soil samples were obtained from the grinding and subsequent packing of the UD soil samples, so that differences in soil characteristic and permeability functions were solely due to soil structure. The elimination of soil structure of the D samples changed the soil water retention parameters, b and λ, consistently with the disappearance of macropores. In the high matric pressure head (more negative), the influence of structure disappeared. The air and water permeability values of UD samples were significantly higher than the D soil samples, due to the major role of soil structure and macropore flow on permeability. Analysis of tortuosity effects showed the presence of a threshold value for the UD soils, defined as the saturation value at which permeability changes abruptly. This is consistent with the presence of macropores that affects pore connectivity for either fluid. Our data confirm that the tortuosity-connectivity parameter, *l*, cannot be used interchangeably between air and water permeability. The relation between l_1 (water permeability) and l_2 (air permeability) is largely controlled by soil structure. In summary, when using permeability models, we must be careful to distinguish between disturbed and undisturbed soils.

ACKNOWLEDGMENTS

The research was partly funded by the Kearney Foundation of Soil Science and the Agricultural Systems Program of the USDA.

REFERENCES

Ball, B.C. 1981a. Modeling of soil pores as tubes using gas permeabilities, gas diffusivities and water release. J. Soil Sci. 32:465–481.

Ball, B.C. 1981b. Pore characteristics of soils from two cultivation experiments as shown by gas diffusivities and permeabilities and air-filled porosities. J. Soil Sci. 32:483–498.

Bear, J. 1972. Dynamics of fluids in porous media. Dover Publications, Inc., New York.

Blackwell, P.S., A.J. Ringrose-Voase, N.S. Jayawardane, K.A. Olsson, D.C. Mckenzie, and W.K. Mason. 1990. The use of air-filled porosity and intrinsic permeability to air to characterize structure of macrospore space and saturated hydraulic conductivity of clay soils. J. Soil Sci. 41:215–228.

Campbell, G.S. 1974. A simple method for determining unsaturated conductivity from moisture retention data. Soil Sci. 117:311–314.

Chen, J., J.W. Hopmans, and M.E. Grismer. 1999. Parameter estimation of two-fluid capillary pressure-saturation and permeability functions. Adv. Water Resour. 22:479–493.

Clennell, M.B. 1997. Tortuosity: A guide through the maze. p. 229–344. *In* M.A. Lovell, and P.K. Harvey (ed.) Developments in petrophysics. Geological Society Spec. Publ. No. 122. Geological Society, London.

Dury, O., U. Fischer, and R. Schulin. 1999. A comparison of relative nonwetting-phase permeability models. Water Resour. Res. 35:1481–1493.

Eching, S.O., J.W. Hopmans, and O. Wendroth. 1994. Unsaturated hydraulic conductivity from transient multi-step outflow and soil water pressure data. Soil Sci. Soc. Am. J. 58:687–695.

Ehlers, W., O. Wendroth, and F. de Mol. 1995. Characterizing pore organization by soil physical parameters. p. 257–275. *In* K.H. Hartge and B.A. Stewart (ed.) Soil structure–Its development and function. Adv. Soil Sci. CRC Press, Boca Raton, FL.

Hillel, D. 1998. Environmental soil physics. Academic Press, San Diego.

Hopmans, J.W., J. Simunek, N. Romano, and W. Durner. 2002. Simultaneous determination of water transmission and retention properties. Inverse methods. p. 963–1008. *In* J.H. Dane and G.C. Topp, (ed.) Methods of soil analysis. Part 4. SSSA Book Series No. 5. SSSA, Madison, WI.

Hunt, A.G., and G.W. Gee. 2002a. Application of critical path analysis to fractal porous media: Comparison with examples from Hanford site. Adv. Water Resour. 25:129–146.

Hunt, A.G., and G.W. Gee. 2002b. Water-retention of fractal soil models using continuum percolation theory: Tests of Hanford site soils. Vadose Zone J. 1:252–260.

Hunt, A.G. 2004. Continuum percolation theory for water retention and hydraulic conductivity of fractal soils: Estimation of the critical volume fraction for percolation. Adv. Water Resour. 27:175–183.

Iversen, B.V., P. Moldrup, P. Schjønning, and P. Loll. 2001. Air and water permeability in differently textured soils at two measurement scales. Soil Sci. 166:643–659.

Janse, A.R.P., and G.H. Bolt. 1960. The determination of the air-permeability of soils. Nether. J. Agr. Sci. 8:124–131.

Klute, A., and A. Dirksen. 1986. Hydraulic conductivity and diffusivity: Laboratory methods. p. 687–734. *In* A. Klute (ed.) Methods of soil analysis. Part 1. Agron. Monogr. No 9. ASA and SSSA, Madison, WI.

Luckner, L., M.Th. van Genuchten, and D.R. Nielsen. 1989. A consistent set of parameteric models for the two-phase flow of immiscible fluids in the subsurface. Water Resour. Res. 25:2187–2193.

Miller, C.T., G. Christakos, P.T. Imhoff, J.F. McBride, J.A. Pedit, and J.A. Trangenstein. 1998. Multiphase flow and transport modeling in heterogeneous porous media: Challenges and approaches. Adv. Water Resour. 21:77–120.

Moldrup, P., T.G. Poulsen, P. Schjønning, T. Olesen, and T. Yamaguchi. 1998. Gas permeability in undisturbed soils: Measurements and predictive models. Soil Sci. 163:180–189.

Moldrup, P., T. Olesen, T. Komatsu, P. Schjønning, and D.E. Rolston. 2001. Tortuosity, diffusivity, and permeability in the soil liquid and gaseous phases. Soil Sci. Soc. Am. J. 65:613–623.

Moldrup, P., S. Yoshikawa, T. Olesen, T. Komatsu, and D.E. Rolston. 2003. Air permeability in undisturbed volcanic ash soils: Predictive model test and soil structure fingerprint. Soil Sci. Soc. Am. J. 67: 32–40.

Mualem, Y. 1976. A new model for predicting the hydraulic conductivity of unsaturated porous media. Water Resour. Res. 12:513–522.

Schaap, M.G., and F.J. Leij. 2000. Improved prediction of unsaturated hydraulic conductivity with the Mualem-van Genuchten Model. Soil Sci. Soc. Am. J. 64:843–851.

Schjønning, P., L.J. Munkholm, P. Moldrup, and O.H. Jacobsen. 2002. Modeling soil pore characteristics from measurements of air exchange: The long term effects of fertilization and crop rotation. Eur. J. Soil Sci. 53:331–339.

Singer, M.J. 1986. Sample preparation. p. 8–9. *In* M.J. Singer and P. Janitzky (ed.) Field and laboratory procedures used in a soil chronosequence study. U.S. Geological Survey Bulletin No. 1648. U.S. Gov. Print. Office, Washington, DC.

Tuli, A., K. Kosugi, and J.W. Hopmans. 2001a. Simultaneous scaling of soil water retention and unsaturated hydraulic conductivity functions assuming lognormal pore-size distribution. Adv. Water Resour. 24:677–688.

Tuli, A., M.A. Denton, J.W. Hopmans, T. Harter, and J.L. MacIntyre. 2001b. Multi-step outflow experiment: From soil preparation to parameter estimation. Department of Land, Air, and Water Resources Pap. No 100037. University of California, Davis, CA.

Tuli, A., and J.W. Hopmans. 2004. Effect of degree of fluid saturation on transport coefficients in disturbed soils. Eur. J. Soil Sci. 55: 147–164.

Vervoort, R.W., and S.R. Cattle. 2003. Linking hydraulic conductivity and tortuosity parameters to pore space geometry and pore-size distribution. J. Hydrol. (Amsterdam) 272:36–49.

Vogel, H.J. 1997. Morphological determination of pore connectivity as a function of pore size using serial sections. Eur. J. Soil Sci. 48: 365–377.

Vogel, H.J. 2000. A numerical experiment on pore size, pore connectivity, water retention, permeability, and solute transport using network models. Eur. J. Soil Sci. 51:99–105.

Wraith, J.M., and D. Or. 1998. Nonlinear parameter estimation using spreadsheet software. J. Nat. Resour. Life Sci. Edu. 27:13–19.

Wildenschild, D., J.W. Hopmans, M.L. Rivers, and A.J.R. Kent. 2005. Quantitative analysis of flow processes in a sand using synchrotron x-ray microtomography. Vadose Zone J. 4:112–126.